Available online at www.sciencedirect.com
ScienceDirect
Marine Chemistry 108 (2008) 1 – 17
MARINE CHEMISTRY
www.elsevier.com/locate/marchem

# Shoreline and seafloor fluxes of water and short-lived Ra isotopes to surface water of San Pedro Bay, CA

Steven L. Colbert *, Douglas E. Hammond

*Dept. of Earth Sciences, University of Southern California, Los Angeles, CA 90089-0740, United States*

Received 16 February 2007; received in revised form 1 September 2007; accepted 5 September 2007
Available online 12 September 2007

**Abstract**

Quantifying Ra inputs to the coastal ocean is an important constraint for using Ra isotopes as a tracer of nearshore mixing in the water column. A study of the short-lived Ra ($^{223}$Ra, $^{224}$Ra) inputs from the seafloor and shoreline to the surface water of San Pedro Bay is presented. The Ra flux is a function of the seawater flux through sediments. Three different water exchange mechanisms were examined. At the shoreline, tides generated water table fluctuation and pump 3.3 $m^3$ $d^{-1}$ (m shoreline)$^{-1}$ of water through the beach, with a residence time of about a day based on the ingrowth of Rn and Ra. Waves pump a model-derived estimate 6.4 $m^3$ $d^{-1}$ (m shoreline)$^{-1}$ of water through the beach face. On the seafloor, waves and currents interacting with ripples generate pressure gradients that drive seawater circulation through sediments. A model fit to a Rn profile indicated that the top 28 cm of pore water exchanges 25% per day with the overlying water. Applying these parameters, the model also produced a reasonable fit to Ra pore water profiles. Extrapolating this rate across the seafloor in contact with the mixed layer, 32 $m^3$ $d^{-1}$ (m shoreline)$^{-1}$ of water is pumped through the seafloor. Combined, a total of 42 $m^3$ $d^{-1}$ (m shoreline)$^{-1}$ of surface water is pumped through sediments.

Using these water exchange rates and pore water measurements of $^{223}$Ra and $^{224}$Ra, the Ra flux from the shoreline and seafloor were computed. Only 5% of the short-lived Ra originates at the shoreline, while the seafloor accounts for 95% of the inputs to the surface mixed layer. A Ra budget for San Pedro Bay surface mixed layer was developed. For $^{224}$Ra, inputs were balanced by radioactive decay. But for $^{223}$Ra, an onshore flow of low-Ra water is required to balance the isotope budget. Using the short-lived Ra isotope data, the maximum residence time of water in San Pedro Bay is 18±10 days.


*Keywords:* Radon; Radium; Coastal ocean; Permeable sediments; Beach; Circulation; USA; CA; San Pedro Bay; Huntington Beach

## 1. Introduction

Large volumes of water are pumped through permeable sediments on continental shelves, driven by currents, tides and gravity waves (Emery and Foster, 1948; Huettel and Webster, 2001; McLachlan, 1982; Riedl, 1971; Riedl et al., 1972). Macroscopic organisms also actively pump water through sediments (see review by Aller, 2001). Water entering the sediments carries oxygen and organic matter, both fine-grained and dissolved, which are consumed by bacteria and returned to the water column as dissolved $CO_2$ and nutrients (Huettel and Rusch, 2000). The importance of permeable

* Corresponding author. School of Oceanography, Box 355351, University of Washington, Seattle, WA 98195, United States. Tel.: +1 206 543 0744; fax: +1 206 685 3351.
*E-mail address:* scolbert@alumni.usc.edu (S.L. Colbert).

0304-4203/$ - see front matter © 2007 Elsevier B.V. All rights reserved.
doi:10.1016/j.marchem.2007.09.004

sediments in global biogeochemical cycles is just beginning to be constrained. However, measuring the flux of solutes across the interface between the water column and permeable sediments is not trivial because traditional methods are not applicable (Jahnke et al., 2000). Several advances have been made in measuring the flux of water and solutes through permeable sediments from both laboratory and field experiments (see review by Huettel and Webster, 2001).

In this paper, we present sediment-water exchange rates based on the deficiency of $^{222}$Rn in pore water. Rn has long been recognized as a tracer of sediment-water exchange (Broecker, 1965). Rn ($t_{1/2}$=3.8 d) is a naturally-occurring, radioactive noble gas that is produced by the decay of the long-lived isotope, $^{226}$Ra ($t_{1/2}$=1600 y). $^{226}$Ra is generally associated with sediments, which produces high activities of Rn in pore water. Advection of low-Rn bottom water through the seafloor generates a pore water activity concentration that is less than can be sustained by the production rate. This difference can then be used to calculate the exchange rate. Similarly, the four Ra isotopes are each produced by a Th parent. Th has a low solubility and is either adsorbed to sediments or incorporated in the mineral structure. $^{223}$Ra ($t_{1/2}$=11.4 d) and $^{224}$Ra ($t_{1/2}$=3.66 d) have half-lives that are comparable to Rn and should also be useful in measuring sediment-water exchange rates (Hancock et al., 2000; Rama and Moore, 1996). $^{228}$Ra ($t_{1/2}$=5.8 y) might also be useful, but on longer time scales. Unlike Rn, dissolved Ra will adsorb to sediments, particularly those with high surface areas, such as manganese oxides.

Our interest in short-lived Ra goes beyond sediment-water exchange rates. These isotopes may also be useful for measuring rates of cross-shelf mixing in the coastal ocean. Once a parcel of water is isolated from its seafloor source, the Ra activity will decrease by radioactive decay and dilution with "older" low-Ra water. The distribution of a Ra isotope reflects the transport that has occurred during the mean life of the isotope, as well as the isotope source function. To calculate the mixing rate, previous studies relied solely on Ra measurements from the water column (Moore, 2000b; Torgersen et al., 1996). These studies assumed that the observed water column Ra inventory was equal to the inputs and that longshore changes in sources and sinks of Ra were negligible. A more complete analysis of coastal ocean sources and sinks of Ra is needed to assess the validity of these assumptions. Furthermore, characterizing the Ra source function places an important constraint on mixing models based on the Ra distribution.

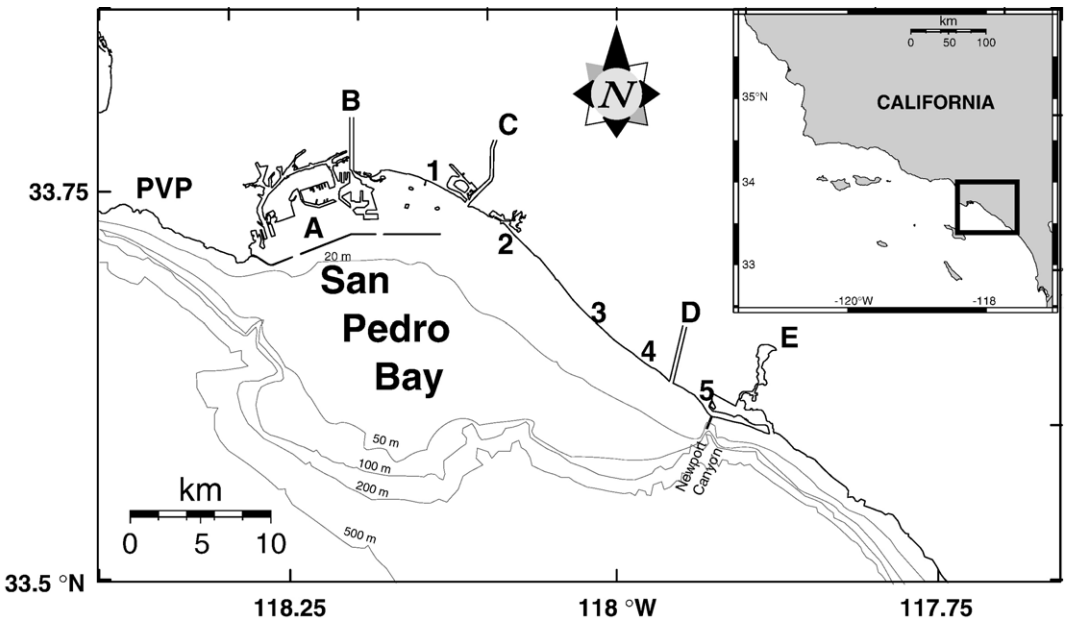


Fig. 1. Map of San Pedro Bay, CA. Inset shows regional map of southern California. Santa Catalina Island is at bottom-left corner of box in the inset. Bodies of water: A=Ports of Los Angeles and Long Beach, B=Los Angeles River, C=San Gabriel River, D=Santa Ana River, E=Newport Bay. Cities and sample locations: 1=Long Beach, 2=Sunset Beach, 3=Huntington Beach, 4=Huntington State Beach, 5=Newport Beach, PVP=Palos Verdes Peninsula.

In this paper, the processes that regulate the release of short-lived Ra from the sea floor to the surface mixed layer at Huntington Beach, CA, are examined. Short-lived Ra inputs are divided into two sources, shoreline and seafloor, and the Ra flux from each was assessed. Computing the Ra flux required knowing the rate water circulates through the sediments, which was also computed. Finally, to obtain information on the residence time of water in the coastal ocean, the Ra input fluxes are compared with measurements of the offshore surface water inventory (Colbert, 2004).

## 2. Study site

San Pedro Bay is a relatively broad (width = 20 km) continental shelf located near the middle of the Southern California Bight (Fig. 1), bounded by Palos Verdes Peninsula and Newport Canyon. At the north end of the bay, a 14 km breakwall extends east from Palos Verdes and protects the Harbors of Los Angeles and Long Beach. San Pedro Bay is naturally sheltered from the north by the Palos Verdes Peninsula and the southwest by Santa Catalina Island. Waves approach the Bay through corridors from the west and south (Gorsline and Grant, 1972). During the summer, the largest waves are associated with the southern swell, produced by storms in the South Pacific (Horrer, 1950).

Three rivers discharge into the Bay: the Los Angeles, San Gabriel, and Santa Ana Rivers. During the warm, dry summer, most of the river water is diverted upstream to recharge groundwater. Below these diversions, the rivers have a minor flow composed of dry-weather runoff, treated domestic sewage, and industrial discharges. During the wet, mild winter, these rivers are the primary source of sediments to San Pedro Bay (Emery, 1960).

San Pedro Bay beach sands are primarily arkose, with heavy minerals dominated by hornblende (Emery, 1960). The mean grain size of beach sand is 250 μm and changes slightly with environmental conditions (Bascom, 1951; Magnusen, 1995). At 1 km offshore, mean grain size decreases from >250 μm in the north part of the bay to <60 μm offshore from the Santa Ana River (Grant, 1973; Moore, 1951). At Huntington Beach, the beach slope is between 1/12 and 1/20.

Tides in Southern California are mixed, with two high tides and two low tides of unequal height. The mean tidal range is approximately 1.1 m; during spring tides, the range exceeds 2 m. Across much of the shelf, major tidal currents flow parallel to the shoreline, propagate to the north and have strong oscillatory motions that result in little net movement over a tidal cycle (Karl et al., 1980; Noble et al., 2003).

## 3. Methods

### 3.1. Tidal wedge volume

The water table elevation at Huntington State Beach was monitored during a flood tide using 5 piezometers (4 cm screened interval) installed perpendicular to the shoreline. The well heights were referenced to each other using a water level, with an uncertainty of ±0.5 cm. The distance between the top of the well and the water table was measured by lowering an electrode until it contacted water, with an uncertainty of ±0.3 cm.

### 3.2. Radium analysis

Within 4 days of collection, $^{223}$Ra and $^{224}$Ra adsorbed to the acrylic fibers impregnated with manganese dioxide (Mn-fibers) (Moore, 1976) were analyzed using a flow-through system with a scintillation detector linked to a time-delayed coincidence counter (RaDeCC) that can distinguish the decays of the Ra daughters, $^{219}$Rn and $^{220}$Rn, which rapidly grow into equilibrium with their parents (Moore and Arnold, 1996). Measured activities were corrected for decay and $^{224}$Ra ingrowth from $^{228}$Th that also adsorbed to the fibers. Internal standards and those prepared from EPA monazite and pitchblende standards were used to compute the absolute activities of each isotope. Analytical errors reported are ±1 standard deviation based on counting statistics.

### 3.3. Slurry experiment-emanation and adsorption characteristics of sands

To compute the $^{223}$Ra and $^{224}$Ra emanation rates and distribution coefficient, sequential aliquots of water were removed from a sediment slurry. About 300 g of surface sand (0–2 cm) was collected and stored wet for a month or more to allow these isotopes to approach secular equilibrium. The slurry was made by adding 1000 g of surf zone seawater that lacked $^{223}$Ra and $^{224}$Ra (by either aging >2 months or passing through a Mn-fiber filter). The slurry was stirred for 10 min at 22 °C to reach sorption equilibrium (Krishnaswami et al., 1982). Afterwards, the supernatant water was decanted and filtered (Whatman #1 filter paper) if fine-grained particles remained suspended. Equal volumes of water were added and removed a total of 4 times. Ra was extracted by passing the water through a Mn-fiber filter. The short-lived Ra isotopes were measured using RaDeCC. Ra ingrowth was negligible during the 90 min required to perform this experiment.

### 3.4. Incubation experiment

Saturated beach sands were incubated to allow short-lived Ra and Rn to grow into equilibrium with sediment emanation. About 12 L of wet, swash zone (<10 cm deep) sands were collected at 5 beaches between Long Beach and San Clemente. In the laboratory, each sample was homogenized and seawater

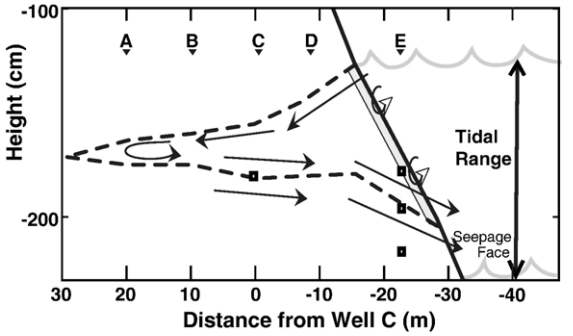


Fig. 2. Cross section of shoreline at Huntington State Beach. The vertical axis is measured from the beach surface (solid line) at Well C. Tidal wedge volume (dotted lines) was defined by the maximum and minimum water table elevation in each well, demarked by letters across the top. Open boxes represent the location of pore water samples. In general, water enters the beach during high tide and drains out during low tide (solid arrows). Some mixing also occurs within the beach. Shaded box at beach surface represents the volume that is affected by wave pumping (open arrows).

aged >2 months from the Huntington Beach surf zone was added to saturate the samples, leaving about 3 cm of water at the surface. The samples were incubated for at least 16 days to allow $^{224}$Ra to reach secular equilibrium. The contribution of initial adsorbed and pore water $^{224}$Ra to the concentration calculation is negligible. Initial $^{223}$Ra may result in over-estimating the $^{223}$Ra concentration by less than 5%, which is within the uncertainty based on the counting statistics. Using a piezometer, 520 ml of water was extracted with a syringe and passed through a Mn-fiber filter to extract Ra. The short-lived Ra isotopes were measured using RaDeCC.

Separate incubations were made to measure Rn emanation rate. A slurry of 20 cm$^3$ of sand and 100 ml of seawater was flushed with helium to remove initial Rn and sealed. After incubating for at least two weeks, the Rn was stripped out of the sample and analyzed (Mathieu et al., 1988). For each sample, emanation measurements were repeated until the standard deviation was less than 5%. For muddy sediments, the slurry porosity is greater than the in situ porosity, which allows greater Rn emanation (Hammond and Fuller, 1979). But for sands, the change in porosity and any difference between experimental and in situ emanation was assumed to be negligible.

### 3.5. Pore water sampling and analysis

At Huntington State Beach, pore water samples were collected at the shoreline and offshore at 7.3 m and 8.5 m water depth. SCUBA divers accessed the two offshore stations from the shoreline. The 7.3 m station was 125 m offshore and just outside the surf zone. The 8.5 m station was 250 m offshore, the maximum distance the divers could safely swim. Pore waters were collected using a piezometer, 0.64 cm OD steel tubing with a 2 cm screened interval. To stabilize the piezometer and impede vertical flow during sampling, the piezometer passed through the center of a plastic plate (radius = 15 cm) that rested on the seafloor. Samples were drawn from average depths of 8, 28, 48, and 78 cm. After inserting the piezometer, 100 to 200 ml of water were drawn by syringe to flush and develop the well. Samples were then drawn into evacuated 0.5 L glass bottles. Assuming laminar, radial flow, water should be extracted from a 15 cm radius around each well. Samples were analyzed for Rn (Mathieu

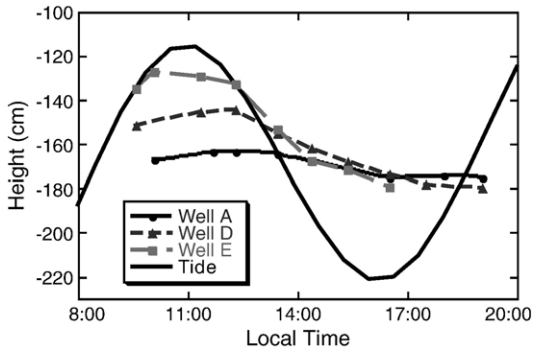


Fig. 3. Well hydrographs at Huntington State Beach compared to the tide on 8/28/03. All water heights are relative to the beach surface at Well C. Inset shows tidal height during 24-hour period.

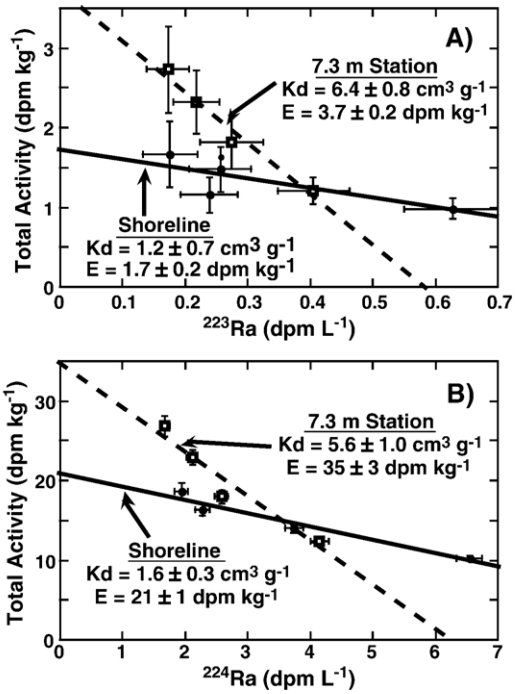


Fig. 4. Results of adsorption experiment, A) $^{223}$Ra and B) $^{224}$Ra. Circles and solid lines are for beach sands and squares and dashed lines are for sand at 7.3 m station.

et al., 1988), and then passed through a Mn-fiber filter to extract Ra.

### 3.6. Porosity

The porosity of surface sediment from the Huntington Beach swash zone and 7.3 m station was measured. For each, 250 $cm^3$ of dry sand was placed in a flask, and seawater was slowly added from the bottom. Dividing the volume of water added to the total volume of sediment gave the porosity, 0.40±0.02. Duplicate measurements were made to test for any packing effect. The volume of pore space through which flow can occur, excluding water retained by surface tension and water in non-interconnected and dead-end pores, was measured on Huntington Beach swash zone sands, using 250 $cm^3$ of dry sand packed in a column. The sand was saturated with seawater and allowed to drain for six hours. The effective porosity is the ratio of the volume of water recovered to the bulk sediment volume, 0.10±0.02.

## 4. Results

### 4.1. Tidal pumping

The rise and fall of the tide pumps water through the beach face (Fig. 2). Sea water infiltrates the beach when the sea surface, which depends on the tides and wave run-up, is higher than the beach water table. A seaward hydraulic gradient drives a reciprocal flow out of the beach during low tide. Tidal oscillations of the water table were observed (Fig. 3). The influence of tides on the beach water table extended >30 m landward of the high tide mark. Moving inland, the amplitude of the tidal fluctuations decreased and the tidal lag increased. The volume of water exchanged during a tidal cycle was calculated by integrating between the maximum and minimum water table elevations (Fig. 2) and multiplying by the effective porosity. For the observed tidal cycle, the volume of water pumped through the beach was 1.4±0.2 $m^3$ (m shoreline)$^{-1}$. Assuming the tidal wedge volume scales linearly with the tidal height, the average daily flux of water through the beach due to tides is 3.3±0.5 $m^3$ $d^{-1}$ (m shoreline)$^{-1}$. This flux is similar to modeled estimates of the tidal pumping flux (Boehm et al., 2006).

### 4.2. Slurry experiment results

A slurry experiment was used to measure the Ra distribution coefficient ($K_d$, $cm^3$ $g^{-1}$) and the emanation rate ($E$, atoms $min^{-1}$ $g^{-1}$), the rate mobile isotopes (those that are available for transport in pore water) are produced. An emanation rate for each Rn and Ra isotope was calculated. Mobile Ra is either dissolved in pore fluid ($\lambda C$, dpm $cm^{-3}$) or adsorbed to sediments ($\lambda C'$, dpm $g^{-1}$). These two pools are related by the distribution coefficient: $K_d = \lambda C'/\lambda C$. In this experiment, surface sands collected at the shoreline and 7.3 m water depth were used. A slurry, formed by adding a known mass of dry sand ($M_s$) to a defined volume of seawater ($V_T$), was stirred to equilibrate the adsorbed and dissolved phases. The activity concentration in the dissolved phase ($\lambda C_i$) was measured by removing an aliquot of water ($\Delta V$). After each removal $\Delta V$, an equivalent volume of Ra-free seawater was returned to the slurry to maintain the volume $V_T$. This procedure was repeated several times using additional aliquots of $\Delta V$. After removal step $i-1$ and adding $\Delta V$, the dissolved Ra remaining in the slurry ($\lambda C_i$) is:

$$(V_w + K_d M_s)\lambda C_i = EM_s - \Delta V \sum \lambda C_{i-1} \quad (1)$$

Where $\Delta V \Sigma \lambda C_i$ is the total Ra removed from the slurry. Eq. (2) was expanded and rearranged so that $K_d$ is the slope and $E$ is the $y$-intercept:

$$\frac{1}{M_s}\left(\Delta V \sum \lambda C_{i-1} + V_T \lambda C_i\right) = -K_d \lambda C_i + E \quad (2)$$

This linear relationship was plotted for each isotope (Fig. 4). The $K_d$ computed from the $^{223}$Ra and $^{224}$Ra data were not

Table 1
Analysis of surface sands (0–2 cm) from Huntington State Beach collected Sept. 11, 2003

| | Beach sand | 7.3 m station | 8.5 m station |
|---|---|---|---|
| Fraction of fines (<180 μm) | 11% | 70% | 76% |
| Porosity | 0.40±0.02 | 0.40±0.02 | |
| *Total sediment activity concentration* (*dpm kg$^{-1}$*) | | | |
| $^{226}$Ra | 1090±60 | 1300±50 | 2470±290 |
| $^{224}$Ra | 1840±80 | 1760±70 | 4120±90 |
| $^{228}$Ra | 1970±180 | 1930±140 | 4380±190 |
| *Emanation rate* (*dpm kg$^{-1}$*) | | | |
| $^{222}$Rn | 46±2 | 57±2 | 83±2 |
| $^{223}$Ra | 1.7±0.2 | 3.7±0.2 | |
| $^{224}$Ra | 21±1 | 35±3 | |
| *Emanation efficiency* (*emanation rate/total sediment concentration*) | | | |
| $^{222}$Rn | 4.2±0.2% | 4.4±0.2% | 3.4±0.1% |
| $^{223}$Ra[a] | 3.3±0.4% | 5.7±0.9% | |
| $^{224}$Ra | 1.1±0.1% | 2.0±0.1% | |
| *Adsorption*[b] | | | |
| Distribution Coefficient ($K_d$) ($cm^3$ $g^{-1}$) | 1.6±0.3 | 5.6±0.6 | |
| Equilibrium partition coefficient ($K_p$) | 6.0±1.1 | 21.0±2.3 | |
| *Predicted PW concentration*[c] (*dpm L$^{-1}$*) | | | |
| $^{222}$Rn | 172±6 | 214±7 | 310±9 |
| $^{223}$Ra | 0.9±0.2 | 0.6±0.1 | |
| $^{224}$Ra | 11±2 | 5.9±0.9 | |

Weight percent of sediments finer than 180 μm, total sediment activities, emanation rates, Ra adsorption coefficients, and predicted equilibrium pore water concentration.
[a]Estimated assuming $^{238}$U/$^{235}$U=$^{226}$Ra/$^{223}$Ra=21.
[b]Based on $^{224}$Ra data in Fig. 4.
[c]Computed using Eq. (3).

Table 2
Huntington State Beach pore water measurements: A) shoreline samples and B) offshore samples

| Depth below surface (cm) | Distance from shore (km) | Concentration in dpm $L^{-1}$ | | | Pore water age in days | | |
|---|---|---|---|---|---|---|---|
| | | $^{222}$Rn | $^{223}$Ra | $^{224}$Ra | $^{222}$Rn | $^{223}$Ra | $^{224}$Ra |
| *A) Horeline samples* | | | | | | | |
| 8 | 0 | 20.5±1.0 | 0.70±0.10 | 11.8±0.7 | 0.74±0.04 | 1.7±0.3 | 3.3±0.2 |
| 28 | 0 | 0.3±0.3 | 0.17±0.05 | 3.6±0.3 | 0.004±0.004 | 0.2±0.1 | 0.2±0.0 |
| 48 | 0 | 61.4±1.3 | 0.64±0.16 | 9.2±0.6 | 3.0±0.1 | 1.5±0.4 | 1.3±0.1 |
| 78 | 0 | 134±1 | 1.20±0.19 | 12.9±0.6 | 19.4±2.2 | 7.2±1.1 | 6.5±0.3 |
| 180[a] | 0 | – | 1.16±0.09 | 12.2±0.7 | – | 6.2±0.5 | 4.1±0.2 |
| Average of 0–48 cm | | 27.4±31.1 | 0.50±0.28 | 8.2±4.2 | 1.0±1.2 | 1.0±0.6 | 1.0±0.5 |
| Incubation experiment | | – | 1.59±0.12 | 14.4±0.9 | | | |
| Predicted equilibrium activity conc.[b] | | 172±6 | 0.9±0.2 | 11±2 | | | |
| *B) Offshore samples* | | | | | | | |
| 8 | 0.18 | 68±1 | 1.06±0.24 | 11.4±0.7 | | | |
| 8 | 0.23 | 69±1 | 0.64±0.14 | 8.5±0.5 | | | |
| 28 | 0.18 | 58±1 | 0.74±0.25 | 15.2±1.1 | | | |
| 28 | 0.23 | 145±3 | 0.89±0.16 | 10.7±0.5 | | | |
| 48 | 0.18 | 153±3 | 1.22±0.26 | 15.9±0.9 | | | |
| 78 | 0.18 | – | 1.21±0.17 | 14.3±0.5 | | | |

All samples collected on Sept. 11, 2003, except where noted. The pore water age in the beach was computed using Eq. (9) and $K_p$=6.0 for Ra.
[a]Collected 8/28/03.
[b]Computed in Table 1 using Eq. (3).

significantly different, despite the large uncertainty for the individual $^{223}$Ra measurements. A higher $K_d$ at the 7.3 m station than at the shoreline suggests an offshore increase in sediment surface area, due either to the observed decrease in grain size (Table 1) or possibly to changes in mineralogy.

For each Ra isotope, $E$ was computed from the $y$-intercept of Eq. (2). For Rn, E was measured by incubating a known mass of sediment in a jar and measuring the Rn after achieving equilibrium (Table 1). For all three isotopes, the emanation rate was higher at the 7.3 m station than at the shoreline. The smaller grain size present at 7.3 m should allow more Ra and Rn to escape, causing an increase in $E$. However, the emanation rates observed at both sites are far greater than predicted from the grain size. The relatively high emanation efficiencies may represent enrichment of parent isotopes near grain boundaries (Krishnaswami and Seidemann, 1988) or the presence of nanopores (Rama and Moore, 1984).

The equilibrium pore water activity concentration ($\lambda C_{eq}$) was calculated using results of the slurry experiment. This is a balance between the supply from emanation, sorption to sediments, and radioactive decay:

$$\lambda C_{eq} = \frac{(1-\phi)\rho E}{\phi(1+K_p)} \quad (3)$$

where $\phi$ is total porosity, $\rho$ is the assumed sediment density (2.6 g $cm^{-3}$) and the equilibrium partition coefficient is $K_p = \rho(1-\phi)K_d/\phi$. For the shoreline sands, these $\lambda C_{eq}$ estimates were consistent with $\lambda C_{eq}$ measured directly by incubating sands to allow mobile Ra to grow into equilibrium (Table 2). Between the shoreline and the 7.3 m station, differences in adsorption lead to different $\lambda C_{eq}$ trends for Rn and Ra. For Rn, which was not adsorbed in these low-organic carbon sediments (Wong et al., 1992), both $E$ and $\lambda C_{eq}$ increase at the 7.3 m station (Table 1). But for Ra, both $E$ and $K_p$ were higher at the 7.3 m station than at the shoreline, and $\lambda C_{eq}$ was about 50% smaller.

Table 3
Radium concentrations in nearshore, near bottom water samples offshore from Huntington Beach

| Collection date | Distance above seafloor (m) | Distance from shore (km) | Concentration (dpm $m^{-3}$) | |
|---|---|---|---|---|
| | | | $^{223}$Ra | $^{224}$Ra |
| 9/13/2001 | 0.4 | 1.35 | 4.5±2.3 | 98±9 |
| 4/3/2002 | 1.4 | 1.67 | 9.4±1.4 | 106±4 |
| 6/7/2002 | 2.1 | 1.08 | 11.5±1.2 | 138±4 |
| 6/12/2002 | 0.6 | 0.99 | 11.0±1.1 | 142±4 |
| 8/23/2002 | 0.6 | 0.5 | 15.5±1.2 | 155±3 |
| 6/18/2003 | 0.5 | 0.94 | 19.8±2.1 | 159±5 |
| 6/25/2003 | 0.9 | 1.10 | 23.4±1.8 | 270±6 |
| Average: | | | 13.6±6.5 | 153±57 |

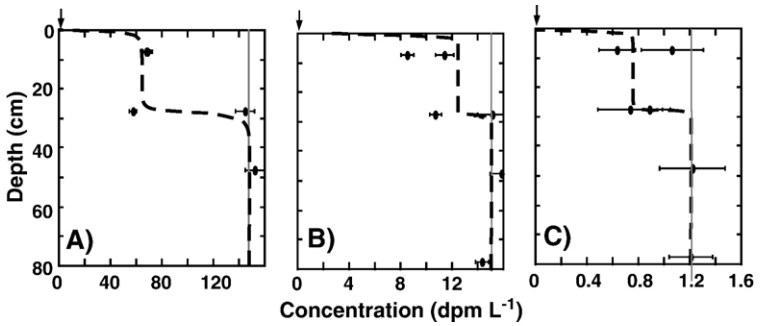


Fig. 5. Pore water concentration composite profiles at 7.5 m and 8.3 m depth offshore of Huntington Beach for A) $^{222}$Rn, B) $^{224}$Ra and C) $^{223}$Ra. Depth uncertainty is equal to the size of the points. Solid line represents the equilibrium pore water activity concentration. Arrow indicates bottom water concentration. In A, dashed line is model fit to data. In B and C, the dashed line is the application of the model to the Ra isotopes.

### 4.3. Pore water data

Pore water was collected at two offshore stations, and composite pore water profiles for Rn, $^{223}$Ra and $^{224}$Ra are presented in Fig. 5. Nearshore bottom water Ra activities were measured on several occasions and averaged 0.014 dpm L$^{-1}$ for $^{223}$Ra and 0.15 dpm L$^{-1}$ for $^{224}$Ra (Table 3). Rn was assumed to be 0.4 dpm L$^{-1}$, twice the concentration measured 25 m offshore at Huntington Beach (Colbert, unpublished data). All three profiles show similar patterns, with a large increase in concentration between the surface and the first sample depth. The greatest variability was found at 28±2 cm depth, suggesting a significant change in concentration near this depth. Below this depth, concentrations remain relatively constant.

## 5. Discussion

### 5.1. Ra budget for San Pedro Bay

With similar wave, tidal, and sediment characteristics along the shoreline of San Pedro Bay, measurements made at Huntington Beach can reasonably be used to estimate regional Ra inputs. Ra is lost from surface water by mixing and radioactive decay. Ra lost by radioactive decay is proportional to the Ra inventory in the mixed layer, which was measured in a series of transects offshore from Huntington Beach (Colbert, 2004). A mass balance for Ra can then be used to evaluate transport in San Pedro Bay.

### 5.2. Shoreline Ra flux

The beach aquifer produces dissolved Ra that is flushed into the surf zone by waves and tides (Fig. 2). The Ra flux from these two processes must be assessed individually, since each occurs at a different rate and length scale. Wave pumping occurs when seawater percolates into the beach as waves run-up onto unsaturated sand and rapidly drains back out of the beach. This shallow, rapid cycling of water strips Ra from a layer of sand extending across the swash zone. If all of the mobile

Table 4
Summary of Ra flux from wave and tide pumping through the beach

| | $^{223}$Ra | $^{224}$Ra | $^{224}$Ra/$^{223}$Ra flux ratio |
|---|---|---|---|
| *Wave flux* | | | |
| Length of swash zone (m) | 22±2 | 22±2 | |
| Depth of wave pumping (m) | 0.20±0.06 | 0.20±0.06 | |
| Porosity | 0.40±0.05 | 0.40±0.02 | |
| Pore water volume (m$^3$ m$^{-1}$) | 1.76±0.59 | 1.76±0.56 | |
| Shoreline emanation rate (dpm kg$^{-1}$) | 1.7±0.3 | 21±2 | |
| Flux (10$^3$ atoms s$^{-1}$ (m shore)$^{-1}$) | 0.19±0.07 | 2.4±0.8 | 12.2±2.7 |
| *Tidal flux* | | | |
| Beach water concentration (dpm m$^{-3}$) | 502±151 | 8175±2452 | |
| Water flux[a] (m$^3$ day$^{-1}$ (m shore)$^{-1}$) | 2.3±0.3 | 2.3±0.3 | |
| Flux (10$^3$ atoms s$^{-1}$ (m shore)$^{-1}$)[b] | 0.32±0.10 | 1.6±0.5 | 5.1±2.1 |

[a]Flux from tidal pumping after subtracting volume of sediments affected by wave pumping.
[b]Convert from atoms s$^{-1}$ m$^{-1}$ to dpm d$^{-1}$ m$^{-1}$ by multiplying $^{223}$Ra flux by 3.65 and $^{224}$Ra flux by 11.6.

Ra produced in this zone is removed, then the wave pumping Ra flux ($J_{WP}$; atoms $s^{-1}$ (m shoreline)$^{-1}$) is:

$$J_{WP} = E\rho(1-\phi)Wz_{wp} \quad (4)$$

The width of the swash zone ($W$) was about 21.5 m, extending from the low tide seepage face to the mean highest high water mark. The depth of wave pumping ($z_{wp}$) was estimated assuming the waves pump water through a wedge-shaped volume of sediment (e.g. Riedl, 1971). Between successive waves, the water table outcrop (the boundary between dull and glimmering sand) migrated about 4 m. For a beach slope of 1/20 and a horizontal water table, waves pump water through the top 20 cm of sediment. Using these values and the beach sand emanation rate ($E$) from the slurry experiment (Table 1), the flux from wave pumping was computed (Table 4). The primary source of uncertainty is the depth of wave pumping, which may vary by 30% (McLachlan, 1979).

The Ra flux from tidal pumping ($J_{TP}$; atoms $s^{-1}$ (m shoreline)$^{-1}$) was computed based on the pore water Ra activity concentration ($\lambda C_{PW}$):

$$J_{TP} = \lambda C_{PW}(V_{TP} - V_{WP})\tau \quad (5)$$

Where $V_{TP}$ is the tidal pumping volume, $V_{WP}$ is the volume of sediments affected by wave pumping ($Wz_{wp}$), and $\tau$ is 1.95 tidal cycles per day (Table 4). The Ra activity concentration of pore water collected from the seaward end of the tidal wedge (Table 2) should be representative of water draining out of the beach. The validity of this assumption is further assessed using a physical model and an estimate of the residence time of water in Section 5.4.

### 5.3. Benthic Ra flux

A two-zone reaction-diffusion-non-local exchange model was developed to compute the water exchange rate and isotope fluxes based on the distribution of Ra and Rn isotopes. In the Upper Zone, complex flow paths are generated as waves and currents interact with ripples on the seafloor, with some regions having net downward flow and others having net upward flow (Huettel et al., 1996; Ziebis et al., 1996). To model this complex pore water transport, we use non-local exchange, a process where a parcel of water at a given depth is exchanged with overlying water at a given rate (Imboden, 1981). Considerable success has been had in using the non-local exchange parameter to describe another complex sediment-water exchange process, bioirrigation (Boudreau, 1984; Emerson et al., 1984, and many subsequent contributions). Non-local exchange may be an appropriate estimate of the exchange rate when

Table 5
Pore water model input parameters and results

| | Symbol | $^{222}$Rn | $^{223}$Ra | $^{224}$Ra |
|---|---|---|---|---|
| *Physical parameters* | | | | |
| Decay constant ($10^{-4}$ $min^{-1}$) | $\lambda$ | 1.26 | 0.42 | 1.32 |
| Porosity | $\phi$ | 0.40 | 0.40 | 0.40 |
| Molecular diffusivity[a] at 18° ($10^{-5}$ $cm^2$ $min^{-1}$) | $D_m$ | 63.0 | 41.4 | 41.4 |
| Adjusted diffusivity[b] ($10^{-5}$ $cm^2$ $min^{-1}$) | $D_s$ | 10.1 | 6.62 | 6.62 |
| *Defined parameters:* | | | | |
| Upper zone thickness (cm) | $L$ | 28 | 28 | 28 |
| Overlying water activity conc. (dpm $L^{-1}$) | $\lambda C_o$ | 1 | 0.014 | 0.15 |
| Ave. irrigated zone conc. (dpm $L^{-1}$) | $\lambda C_i$ | 65 | 0.83 | 10.2 |
| Equilibrium activity conc. (dpm $L^{-1}$) | $\lambda C_{eq}$ | 149 | 1.22 | 15.1 |
| Emanation rate (dpm $kg^{-1}$) | $E$ | 40.0 | 0.8 | 10.5 |
| Distribution coefficient ($cm^3$ $g^{-1}$) | $K_d$ | 0 | 1.4 | 1.4 |
| Partition coefficient | $K_p$ | 0 | 5.3 | 5.3 |
| *Adjustable parameter* | | | | |
| Non-local exchange rate ($10^{-4}$ $min^{-1}$) | $\alpha$ | 1.7 | 1.7 | 1.7 |
| *Results* | | | | |
| Model flux (atoms $m^{-2}$ $s^{-1}$) (±50%) | | −163 | −6.0 | −32.4 |
| Seafloor-mixed layer contact (m) (±15%) | $L_{SF}$ | 1200 | 1200 | 1200 |
| Total flux ($10^3$ atoms $s^{-1}$ $m^{-1}$)[c] (±50%) | $J_{SF}$ | −196 | −7.2 | −39 |

[a]Diffusivity computed based on algorithm presented by Li and Gregory (1974) for Ra, and Jähne et al. (1987) for $^{222}$Rn.
[b]The adjusted diffusivity was computed as $D_s = \phi^2 D_m$ (Ullman and Aller, 1982).
[c]Total flux to mixed layer per m of shoreline.

the pore water concentration is averaged at a given depth. In this study, relatively large pore water samples (0.5 L) effectively integrated pore water within a 15 cm radius around the well. The Upper Zone thickness was defined as 28 cm, because samples at this depth were quite variable, probably indicating an abrupt decrease in non-local exchange. In the Lower Zone, solute transport is assumed to be only by molecular diffusion. The relative importance of molecular diffusion and non-local exchange depends on the isotope half-life, which are relatively similar for Rn and the short-lived Ra isotopes. The model formulation is derived in the Appendix.

Two processes, which may be important in other environments, are not included in this model. First, bioturbation undoubtedly occurs in these sediments. Bioturbation may decrease Ra pore water concentrations and increase the Ra flux from sediments (Hancock et al., 2000; Sun and Torgersen, 2001). However, the bioturbation rate is presumably much slower than the rate at which water is pumped through the sediments. Second, net advection is excluded in this model. During this study, regional hydraulic gradients in aquifers were landward, and seawater intrusion was occurring (Brennan, 2003). In addition, at low flow rates, molecular diffusion and irrigation will dominate the input flux of short-lived Ra (Colbert, 2004). Advection due to sediment accumulation is not important during the mean life of these short-lived isotopes.

The model requires knowing $\lambda C_{eq}$, which can either be calculated (Eq. (3)) or assumed equal to the deep pore water activity concentration. For Rn, the deepest pore water sample was significantly less than $\lambda C_{eq}$ predicted for surface sands (Table 2). For Ra, the opposite was observed, where deep pore water concentrations were greater than $\lambda C_{eq}$ of surface sand (Table 2). If significant pore water exchange was occurring, the deep pore water concentration of both Rn and Ra would decrease relative to $\lambda C_{eq}$. Thus, $\lambda C_{eq}$ of surface and deep sand must be different. Sedimentological studies of the San Pedro Shelf provide insight into this discrepancy. Sediments on the shelf can be grouped into relic and modern end members, along with a range of mixtures (Gorsline and Grant, 1972). The surficial recent sediment is silty, very fine sand with a distinctive gray-green color originating from either the Santa Ana River or the Orange County Sanitation District's sewage outfall (Emery, 1960; Felix and Gorsline, 1971; Grant, 1973). These recent sediments overlie iron oxide-stained relict beach and dune sands and fluvial deposits, which outcrop locally and have a mean grain size similar to beach sand (Felix and Gorsline, 1971; Herndon, 1992; Moore, 1951). It is likely that our deep pore water was drawn from a sediment matrix that is different from surface sediment. Given the similar $\lambda C_{eq}$ of beach sand and the concentration of deep pore water, it is likely these deep sediments are relic beach sand, with $E$ and $K_d$ similar to modern beach sand. We can calculate the Ra adsorption coefficient based on the $\lambda C_{eq}$ of Rn and $^{223}$Ra of relic and beach sand, assuming that the emanation efficiency of the beach and relic sands are the same and that the sediment $^{226}$Ra/$^{227}$Ac ratio is constant. The computed $K_d$ (Table 5) is slightly greater than the beach sand $K_d$, but significantly less than surface sand $K_d$ (Table 1). Then, $E$ for $^{224}$Ra was computed using $K_d$ and the deep pore water concentration. These results suggest that buried relic beach sands have similar U and Th isotope concentrations and ratios as modern beach sands.

The pore water model was fit to the Rn data by adjusting the non-local exchange rate to $1.7\times10^{-4}$ min$^{-1}$ through the top 28 cm of sediments. Since the Rn emanation rate increased near the surface, this exchange rate is a minimum. In comparison to biologically-driven exchange in muddy shelf and estuarine sediments, this non-local exchange rate is relatively high and extends deeper into sediments (Emerson et al., 1984; Townsend, 1997). It is likely this exchange is driven by physical pumping of water driven by waves and currents. The reciprocal of the non-local exchange rate, 4 days, is an estimate of the time required for bottom water to replace this thickness of pore water. The flux of water through the Upper Zone of 27 L m$^{-2}$ d$^{-1}$ can be calculated as the product of the non-local exchange rate and the water volume in the Upper Zone. This water flux is similar to previous estimates of exchange driven by wave pumping through sediments based on computed pressure gradients and dye studies (Mu et al., 1999; Precht and Huettel, 2003; Riedl et al., 1972).

Ra profiles were generated using the computed non-local exchange rate (Fig. 5). The model predicts a rapid increase in concentration in the top few cm, then a relatively constant concentration throughout most of the Upper Zone, where isotope production is balanced by losses to non-local exchange and radioactive decay. At the base of the Upper Zone, the pore water concentration again increases to the equilibrium pore water concentration. The resulting fit to the data was better for $^{223}$Ra than $^{224}$Ra, where the model overestimated the $^{224}$Ra concentration in the upper 28 cm. If $K_d$ in surface sediments is larger than assumed and closer to the observed surficial sediments, the difference between the model and the observed concentrations would be reduced.

Benthic fluxes are presented in Table 5. In this system, the diffusive flux accounts for less than 10% of

the total flux, and is greatest for $^{223}$Ra. Instead, the benthic flux is dominated by the non-local exchange flux. These fluxes can then be used to estimate the seafloor inputs to surface waters.

### 5.4. Surface water budget

Ra inputs measured at Huntington Beach can reasonably be extrapolated along the 19 km of shoreline between Sunset Beach and Newport Beach. Shoreline inputs should be similar because wave, tidal, and sediment characteristics are relatively constant. The uncertainty for each flux increases due to longshore changes in the Ra emanation rate, which is proportional to the total sediment activity concentration (Colbert, 2004). The total sediment activity concentration of swash zone sands varied by less than 30% along this stretch of shoreline (Colbert and Hammond, 2007). Combined with the estimated 30% uncertainty for the depth of wave pumping, and a 30% uncertainty in the effective porosity, the relative uncertainty of each shoreline input flux is 42%.

The seafloor input must be extrapolated both across the shelf and along the shoreline. First, the distance offshore the mixed layer is in contact with the seafloor was calculated. The summertime mixed layer thickness was measured during seven cruises at Huntington Beach, and averaged 12±3 m. Using seafloor bathymetry based on measurements made while sampling and NOAA Nautical Chart 18746, the seafloor area in contact with the mixed layer was 1.2±0.3 km (Colbert, 2004). Second, there is uncertainty in the depth and rate of irrigation, which should vary as a function of water depth, along with the energy associated with waves and currents. These pore water profiles should be representative of the mean, since they were collected near the middle of the mixed layer. Circulation through the sediments is also affected by the presence of ripples (Precht and Huettel, 2003), which form in response to the orbital currents of surface waves. Given the mean summer wave conditions at Huntington Beach, ripples are expected to form to depths greater than 15 m (Denny, 1988), and are observed to depths of 45 m (Drake et al., 1985; Karl et al., 1980; Xu, 2005). The presence of ripples suggests there is not a dramatic decrease with depth in the forces driving circulation through sediments. We estimate that the combined uncertainties in the depth and rate of irrigation contribute a 30% uncertainty to the flux estimate. $K_d$ and $E$ change with distance offshore and longshore (Table 1). These changes appear to be limited to the surface sediments, and are probably not representative of most sediments affected by irrigation. Regardless, when $\lambda C_{eq}$ is held constant and the emanation rate and adsorption are varied within a reasonable range (±50% for $E$, $1<K_d<10$), the flux changes by only 20%. Thus, combined by propagation of errors, the relative uncertainty of the benthic flux calculation is 50%.

The uncertainty of the $^{224}$Ra/$^{223}$Ra input flux ratio is smaller, since this calculation requires fewer parameters (Table 6). For example, the seafloor input flux ratio, and thus its uncertainty, depends on the relative emanation rate, the depth of irrigation, and its rate. The relative Ra emanation rate Between Seal Beach and Newport Beach has a standard deviation of the mean of 6%, assuming emanation is proportional to the total sediment activity concentration (Colbert, 2004). The flux ratio sensitivity to the depth and rate of irrigation is shown in Fig. 7C. At the observed irrigation rate, the flux ratio is fairly insensitive to changes. A 50% change in the irrigation rate changes the flux ratio by only 20%. The ratio is also not very sensitive to the irrigation depth estimate. Based on this sensitivity analysis, the uncertainty of the $^{224}$Ra/$^{223}$Ra seafloor input flux is estimated to be 25%.

In San Pedro Bay surface water, inputs from the shoreline and seafloor must be balanced by losses. If the

Table 6
Summary of A) short-lived Ra inputs to San Pedro Bay measured at Huntington Beach and B) the inventory of short-lived Ra measured in surface water off Huntington Beach, CA, collected between July and September (Colbert and Hammond, 2007)

| | $^{223}$Ra | $^{224}$Ra | $^{224}$Ra/$^{223}$Ra |
|---|---|---|---|
| *A) San Pedro Bay radium inputs input fluxes ($10^3$ atoms $s^{-1}$ (m shoreline)$^{-1}$)*[a] | | | |
| Wave flux ($J_{WP}$) | 0.19±0.08 | 2.4±1.0 | 12.2±2.7 |
| Tide flux ($J_{TP}$) | 0.32±0.13 | 1.6±0.7 | 5.1±2.1 |
| Seafloor flux ($J_{SF}$) | 7.2±3.6 | 39±19 | 5.4±1.1 |
| Total input flux ($J_{Tot}$) | 7.7±3.6 | 43±19.5 | 5.4±1.4b |
| *B) Radium losses by decay ave. surface water inventory ($10^3$ dps (m shore)$^{-1}$)* | | | |
| Huntington Beach transects | 5.1±1.3 | 42±11 | 7.9±1.0 |

[a]To convert from atoms $s^{-1}$ $m^{-1}$ to dpm $d^{-1}$ $m^{-1}$, multiply $^{223}$Ra flux by 3.65 and $^{224}$Ra flux by 11.6.
[b]Uncertainty is dominated by the seafloor flux ratio uncertainty, which we estimated to be 25%.

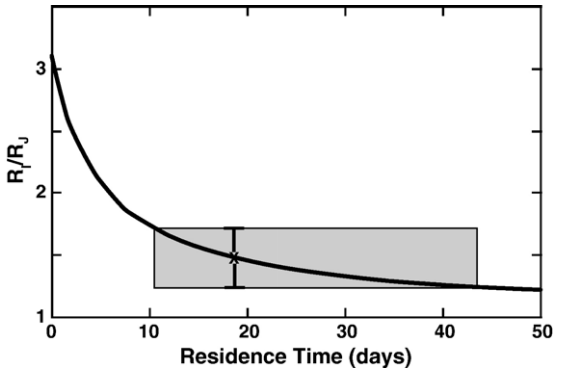


Fig. 6. The ratio of $^{224}Ra/^{223}Ra$ surface water inventory ratio ($R_I$) to $^{224}Ra/^{223}Ra$ input flux ratio ($R_J$) as a function of the residence time of water. The maximum value for the ratio is equal to the $^{224}Ra/^{223}Ra$ decay constant ratio.

residence time of water in San Pedro Bay is sufficiently long (a couple weeks for $^{224}Ra$, more than six weeks for $^{223}Ra$), then there will be no longshore Ra gradient, and the only loss will be by radioactive decay. Ra was measured in transects extending offshore from Huntington Beach during seven summertime cruises (Colbert and Hammond, 2007). Integrating the Ra activity concentration in each transect (i.e. calculating the Ra inventory), the loss of Ra by radioactive decay can be computed.

Comparing the inputs to the loss by radioactive decay (Table 6), $^{223}Ra$ and $^{224}Ra$ input fluxes are within the uncertainty of mean summer surface water inventories at Huntington Beach. However, two pieces of evidence suggest that at least the $^{223}Ra$ is not in equilibrium. First, the $^{224}Ra$ inputs are balanced by losses to radioactive decay, while the $^{223}Ra$ inputs are greater than the losses to radioactive decay. Thus, parameters that affect the input fluxes and are common to both isotopes, like irrigation rate or irrigation depth, cannot be changed to match the inputs to the radioactive decay losses. Stronger evidence that $^{223}Ra$ is not in equilibrium comes from the $^{224}Ra/^{223}Ra$ input ratio, which has a smaller uncertainty. Given enough time to equilibrate, the input flux ratio and the offshore inventory ratio would be the same. Instead, there is an excess of $^{224}Ra$ relative to $^{223}Ra$. These points suggest that the longshore gradient is not negligible, and that the residence time of water in San Pedro Bay is less than the six weeks required for $^{223}Ra$ equilibrium.

An upper limit for the summer residence time of surface water in San Pedro Bay can be estimated using a mass balance for the short-lived Ra isotopes:

$$J_{\mathrm{Tot}}L + Q\,\overline{C}_{\mathrm{in}} = V\lambda\,\overline{C}_{\mathrm{Bay}} + Q\,\overline{C}_{\mathrm{Bay}} \qquad (6)$$

On the left-hand side are the inputs. The first term $J_{\mathrm{Tot}}$ is the sum of the shoreline ($J_{\mathrm{TP}}+J_{\mathrm{WP}}$) and seafloor inputs ($J_{\mathrm{SF}}$) (Table 6). Multiplying these fluxes by the length of shoreline $L$ gives the total input to San Pedro Bay. The second term is for longshore inputs, calculated as the product of the longshore advective flow $Q$ and its average isotope excess activity concentration, $\lambda\overline{C}_{in}$. On the right hand are the losses from radioactive decay and longshore transport, where $V$ is surface water volume, $\lambda$ is the isotope decay constant, and $\lambda\overline{C}_{\mathrm{Bay}}$ is the average excess isotope activity concentration in San Pedro Bay, which can be calculated from the offshore inventory: $I = V\lambda\overline{C}_{\mathrm{Bay}}/L$.

Eq. (7) was written for both isotopes and solved for $J_{\mathrm{tot}}$. Then, taking the $^{224}Ra/^{223}Ra$ ratio of the total input

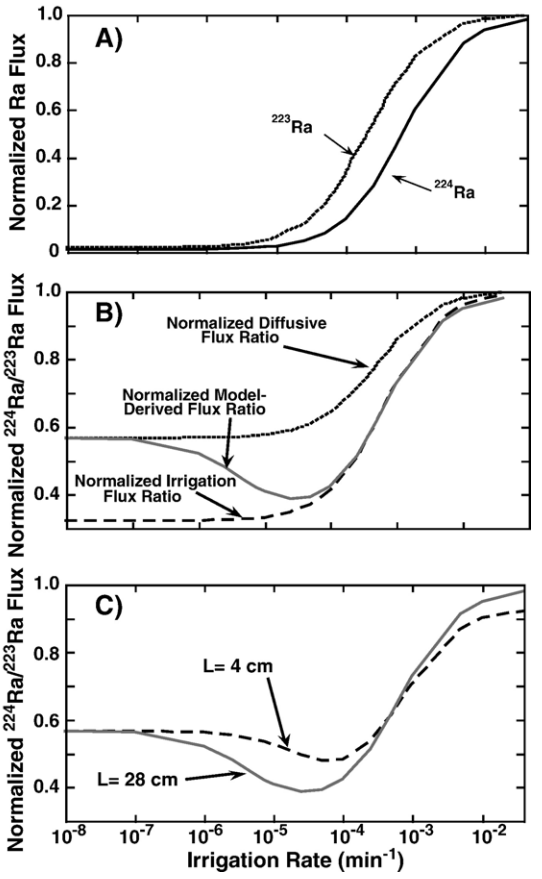


Fig. 7. A) Ra flux normalized to the Ra production rate in the top 28 cm for various irrigation rates. Values used to compute the model-derived flux ratio are presented in Table 5. B) $^{224}Ra/^{223}Ra$ flux normalized to the emanation rate ratio as a function of the irrigation rate. The two components of the flux, the diffusive flux ratio and the irrigation flux ratio, are also shown. C) $^{224}Ra/^{223}Ra$ flux normalized to the emanation rate ratio as a function of the irrigation rate for various Upper Zone thicknesses.

flux ($R_J$), the new equation was rearranged and simplified to calculate the residence time of water in the coastal zone:

$$t = \frac{V}{Q} = \frac{R_\lambda - (R_I/R_J) + R_\lambda \frac{\bar{C}_{223,in}}{\bar{C}_{223,bay}}\left(\frac{R_{in}}{R_J} - 1\right)}{\lambda_{224}[(R_I R_J) - 1]} \quad (7)$$

where $R_\lambda$ is $\lambda_{224}/\lambda_{223}$, $R_I$ is the $^{224}Ra/^{223}Ra$ inventory ratio measured offshore from Huntington Beach, and $R_{in}$ is the unknown longshore input ratio $\bar{C}_{in,224} / \bar{C}_{in,223}$. With this model, we have integrated the concentration offshore in order to examine the age of the water as it flows parallel to the shoreline. This model differs from Moore's (2000a) model, which used the short-lived radium isotope ratio to estimate the age of a costal water mass as it is transported offshore. This model is incompatible with our field site for two reasons. First, Moore's model only allows for inputs at the landward boundary, but at Huntington Beach, seafloor inputs are the primary Ra source. Second, Moore's 1-D model requires no longshore gradient, which is unlikely across San Pedro Bay.

To assess the importance of longshore transport, we assumed that the longshore current is supplied by new water from offshore that enters the coastal zone with no excess $^{224}Ra$ or $^{223}Ra$ $\left(\bar{C}_{223,in} = \bar{C}_{224,in} = 0\right)$. While the location of onshore convergence is not precisely known, it is likely to vary temporally and occur near Sunset Beach, based on the analysis of Colbert and Hammond (2007). This new water appears to be entrained in longshore flow towards the southeast. An equal volume must leave after acquiring Ra.

For Huntington Beach, the $R_I/R_J$ ratio is 1.5±0.3 (Table 6), and the maximum water residence time is 18± 10 days (Fig. 6). Based on current meter measurements, a shorter residence time of about 4 days is estimated (Noble et al., 2003). The residence time estimate from Eq. (7) would be reduced if lateral inputs of Ra are significant ($\bar{C}_{in}$ >0 for both $^{223}Ra$ and $^{224}Ra$). This additional short-lived Ra was provided by the partial entrainment of water derived from north of Sunset Beach (Colbert and Hammond, 2007). To reduce the residence time, the longshore flow isotope concentration ratio must be less than the input flux ratio ($R_{in}$<$R_J$), which requires that the $^{224}Ra/^{223}Ra$ inventory ratio of water entrained in the longshore flow must be less than 16.8. This is consistent with an inventory ratio between 1 for offshore water and 5 for water offshore from Sunset Beach (Colbert and Hammond, 2007). Further constraints on the longshore Ra sources are required to further refine the residence time estimate.

### 5.5. Benthic flux ratio

The relative flux of Ra isotopes provides information on non-diffusive transport of pore water solutes and deserves further discussion. In Fig. 7A, the $^{223}Ra$ and $^{224}Ra$ fluxes, normalized to each emanation rate to generalize this phenomenon, are presented as a function of the non-local exchange rate. As the non-local exchange rate increases, the $^{223}Ra$ flux clearly begins to increase before the $^{224}Ra$ flux. Because of its longer half-life, $^{223}Ra$ is more sensitive to irrigation. This has an interesting impact on the normalized $^{224}Ra/^{223}Ra$ flux ratio (Fig. 7B). For each isotope, the flux has both a diffusive component and an irrigation component, and both are sensitive to the non-local exchange rate (Appendix A). The diffusive component ratio and the irrigation component ratio are also shown in Fig. 7B. At low irrigation rates, diffusion dominates and the flux ratio is equivalent to the diffusive component ratio, $(\lambda_{223}/\lambda_{224})^{0.5}$. At high irrigation rates, the normalized flux ratio approaches 1.0 as all Ra emanated escapes from the seabed. But at moderate irrigation rates (those similar to the isotope decay constants), the differences between the isotopes generates a dip in the normalized $^{223}Ra/^{224}Ra$ flux ratio, with a potential minimum of $\lambda_{223}/\lambda_{224}$ (Appendix A). A normalized flux ratio less than $(\lambda_{223}/\lambda_{224})^{0.5}$ is a unique feature of the non-local exchange model and cannot be generated by other common models, such as enhanced diffusion or 1-D advection-diffusion. By independently measuring the short-lived Ra benthic flux and the emanation rate, the ability of the non-local exchange model to simplify complex transport pathways could be tested.

The flux ratio is also sensitive to the adsorption coefficient, porosity, molecular diffusivity, and the depth of irrigation. Thus, model-derived flux ratios presented in Fig. 7B are only valid for the model values presented in Table 5. Fig. 7C compares the normalized model-derived flux ratio computed for two irrigation depths. Because of the dependence on the isotope half-life, the profile maintains its general shape over a broad range of values.

### 5.6. Tidal wedge residence time

The effective age of water in the tidal wedge can be computed based on the Ra and Rn pore water concentrations. Short-lived Ra and Rn in pore waters are primarily from beach sand emanation. Treating the beach water as a well-mixed system, then the loss of each isotope is by radioactive decay and removal from

the beach. The box model mass-balance equation for each isotope is:

$$V_{TW}\phi(1+K_P)\lambda C_{eq} = V_{TW}\phi(1+K_P)\lambda C_{PW} + \frac{\phi V_{TW}}{\lambda t_b}(\lambda C_{PW} - \lambda C_{SZ}) \quad (8)$$

where $\lambda C_{PW}$ is the pore water activity concentration, $V_{TW}$ is the volume of water in the tidal wedge, $t_b$ is the effective pore water age. The left side of Eq. (8) is the production rate of mobile Ra in the tidal wedge. On the right side, the first term is for radioactive decay, and the second term represents exchange with surf zone water ($\lambda C_{SZ}$). The summer $\lambda C_{SZ}$ averages at Huntington Beach are 0.032 dpm/L and 0.33 dpm/L for $^{223}$Ra and $^{224}$Ra, respectively (Colbert and Hammond, 2007). Surf zone Rn is about 0.15 dpm/L (Colbert, unpub. data). Rearranging and simplifying Eq. (8) to solve for $t_b$:

$$t_b = \frac{1}{\lambda(1+K_p)}\left(\frac{\lambda C_{PW} - \lambda C_{SZ}}{\lambda C_{eq} - \lambda C_{PW}}\right) \quad (9)$$

The location of beach waters collected during the ebb tide are plotted in Fig. 2. Samples had a wide range of computed ages, with the lowest ages for water collected within the top 48 cm (Table 2). The ages from Rn in the upper-most samples were lower than for Ra, which may represent an additional loss by gas exchange. Assuming Ra ages computed in the top 48 cm are representative for water draining out of the tidal wedge, then the residence time of water in the tidal wedge is about 1 day. Deeper samples have much longer residence times, but are not in equilibrium with the sediment emanation rate. This suggests some exchange does occur between the tidal wedge and deeper sediments.

We can estimate the mean residence time of water in the tidal wedge ($\bar{t}_b$) by using a mass balance for a well-mixed reservoir:

$$\bar{t}_b = \frac{V_{TW}}{Q_{TP}} = \frac{\phi}{\tau\phi_e} \quad (10)$$

where $Q_{TP}$ is the rate water is pumped across the beach face. Assuming that the tidal wedge is filled and drained during each tidal cycle, then the water flow rate can be calculated as $Q_{TP} = V_{TW}\phi_e\tau$, where $\tau$ is 1.95 tidal cycles per day. The mean residence time of 2.1±1.1 days is dependant on the ratio of the total porosity to the effective porosity. Given the uncertainty, this estimate is not statistically different from the estimate based on the Rn and Ra data. Further refinement of this model would include circulation through saturated sediments below the tidal wedge, as suggested by the Ra data. This would increase both $\phi_e$ and $V_{TW}$ and reduce the residence time by up to 22% if the volume of sediments flushed is less than three times the tidal wedge volume.

### 5.7. Total water flux

The total flux of water from the mixed layer that is pumped through sediments can be calculated. At the shoreline, water table measurements showed that tides pump 3.3±0.5 m$^3$ d$^{-1}$ (m shoreline)$^{-1}$. Wave pumping was estimated to pump 6.4±1.7 m$^3$ d$^{-1}$ (m shoreline)$^{-1}$ of water, based on the grain size and beach slope (McLachlan, 1982). At the seafloor, the flux of water through the top 28 cm was computed based on modeling the Rn pore water profile. With 1.2±0.3 km of seafloor in contact with the mixed layer, the total flux of water through seafloor sediments is 32±16 m$^3$ d$^{-1}$ (m shoreline)$^{-1}$. Combining these fluxes, the total flow of mixed layer water through sediments was 42±16 m$^3$ d$^{-1}$ (m shoreline)$^{-1}$, with 23% occurring at the shoreline and the rest distributed across the seafloor.

## 6. Conclusions

Several different mechanisms that circulate seawater through permeable sediments were identified. At the shoreline, waves rapidly (minutes to hours) pump water through the top 20 cm of the beach face. Based on a model of wave pumping, the flux of water across the beach face was 6.4 m$^3$ d$^{-1}$ (m shoreline)$^{-1}$.

The rise and fall of the tides generates a hydraulic gradient between sea level and the beach water table. The water table fluctuates with a tidal period that extends more than 30 m inland from the high water mark. Water pumped through the beach by tides was found to have a residence time of about 1 day, based on Ra concentrations in pore water draining out of the beach and a mass balance estimate for water. Ra concentrations in pore waters below the tidal wedge were not fully in equilibrium with the sediment emanation rate, suggesting effects of tidal pumping extend to the sediments below the tidal wedge. Based on water table fluctuations, the flux of water through the beach driven by tides was 3.3 m$^3$ d$^{-1}$ (m shoreline)$^{-1}$.

Along the seafloor, waves and currents interacting with seafloor topography generate pressure gradients that drive a circulation of seawater through the top 28 cm of sediment. This circulation is slower than the wave and tide pumping observed at the shoreline. Using an isotope balance for Rn, these surface sediments are flushed with overlying water every four days. Integrating across the seafloor in contact with the mixed layer,

32 $m^3$ $d^{-1}$ (m shoreline)$^{-1}$ of water was cycled through the seafloor. Combining this seafloor flux with the flux of water through the beach driven by waves and tides, the total flux of surface water through sediments was 42 $m^3$ $d^{-1}$ (m shoreline)$^{-1}$.

Ra inputs from the shoreline and across the seafloor in contact with the mixed layer were calculated. Wave and tide pumping at the shoreline contributed only about 8% of the total short-lived Ra supply. The seafloor in contact with the mixed layer, extending from the shoreline to 1.2 km offshore at Huntington Beach, is the primary source of short-lived Ra. Models that simulate the nearshore Ra distribution to calculate mixing rates will have to include inputs that are distributed across the seafloor in contact with the mixed layer (e.g. Colbert and Hammond, 2007).

Finally, the measurements made at Huntington Beach were extrapolated along the San Pedro Bay shoreline to develop a Ra budget for surface water. The input of $^{224}$Ra was found to be balanced by the losses to radioactive decay. But for $^{223}$Ra, the observed inventory in surface water could only be supported if there was an onshore advection of low-Ra water into San Pedro Bay. The difference between the two isotopes demonstrates the sensitivity of the longer-lived isotope to longshore and onshore advection on the time scale of nearshore mixing in San Pedro Bay. Using the mass balance, the residence time of water in San Pedro Bay must be less than 18 days.

## Acknowledgements

This project was funded by the USC Sea Grant Program, part of the National Sea Grant College Program, National Oceanic and Atmospheric Administration, U.S. Department of Commerce, under grants NA86RG0054 and NA16RG2256, and received additional support from the Wrigley Institute for Environmental Studies and the National Science Foundation grant OCE-0623413. Gerry Smith, Carole Bartel, Shelley Howard, Altay Hammond and Timur Hammond helped with sample collection and analysis. Ra analysis expertise was provided by Ralph Arnold and Billy Moore. This project benefited from discussions with Don Gorsline, Richard Ku, Jed Fuhrman, and Shengde Luo. Notes from four anonymous reviewers were greatly appreciated and used to significantly improved this manuscript.

## Appendix A. Pore water model

A two zone model was developed to compute the water exchange rate and isotope fluxes based on the distribution of Ra and Rn isotopes. The governing equations for each zone of the model at steady state are:

UPPER ZONE: for $0 \le z \le H$,

$$\phi\left(1+K_{\mathrm{p}}\right)\frac{\partial C_u}{\partial t} = \phi D_s \frac{\partial^2 C_u}{\partial z^2} - \phi\alpha(C_u - C_0) - \phi\left(1+K_p\right)\lambda C + \rho(1-\phi)E = 0 \tag{A1}$$

LOWER ZONE: for $z > H$,

$$\phi\left(1+K_p\right)\frac{\partial C_l}{\partial t}\phi D_s \frac{\partial^2 C_l}{\partial z^2} - \phi\left(1+K_p\right)\lambda C_l + \rho(1-\phi)E = 0 \tag{A2}$$

where $C$ is the dissolved isotope concentration in each zone marked with subscript u for upper and l for lower, $C_{\mathrm{o}}$ is the concentration in the overlying water, $t$ is time, $z$ is sediment depth, $H$ is the thickness of the upper zone, $\alpha$ is the non-local exchange rate (1/time), and $\lambda$ is the decay constant (1/time). Net advection is ignored, and exchange of pore water and bottom water is characterized by the parameter $\alpha$. The molecular diffusivity $D_{\mathrm{m}}$ was adjusted for tortuosity, treated as a function of porosity (Ullman and Aller, 1982), to give the effective diffusivity: $D_{\mathrm{s}} = \phi^2 D_{\mathrm{m}}$. Diffusion, $\phi$, $K_{\mathrm{p}}$ and $E$ are assumed to be constant with depth. In the Upper Zone, $\alpha$ is constant. Four boundary conditions are required to solve these differential equations:

$$C_u = C_0 \text{ at } z = 0 \tag{A3}$$

$$C_u = C_l \text{ at } z = H \tag{A4}$$

$$\left(\frac{dC_u}{dz}\right)_{z=H} = \left(\frac{dC_l}{dz}\right)_{z=H} \tag{A5}$$

$$\phi(1+K_P)\lambda C_l = \rho(1-\phi)E \text{ as } z \rightarrow \infty \tag{A6}$$

Briefly, the first boundary condition states that the concentration at the sediment-water interface is equal to the concentration in the overlying water. The second and third conditions produce continuity in total concentration and pore water flux, respectively, between the Upper and Lower Zones. The last condition is that the total mobile concentration at infinite depth is proportional to the isotope emanation rate. The solutions to these differential equations are in the form:

UPPER ZONE : (A7)

For $0 \le z \le H$, $C_u = A_1 e^{rz} + A_2 e^{-rz} + A_3$

LOWER ZONE : (A8)

For $H \le z$, $C_l = B_1 e^{-s(z-H)} + B_2$

Where the scaling parameters are:

$$r = \sqrt{\frac{\alpha + \lambda(K_p + 1)}{D_s}} \tag{A9}$$

$$s = \sqrt{\frac{\lambda(K_p + 1)}{D_s}} \tag{A10}$$

The constants are defined as:

$$A_1 = \frac{B_3 - A_3 - (C_o - A_3)\left(1 - \frac{r}{s}\right)e^{-rH}}{\left(1 + \frac{r}{s}\right)e^{rH} - \left(1 - \frac{r}{s}\right)e^{-rH}} \tag{A11}$$

$$A_2 = C_o - A_1 - A_3 \tag{A12}$$

$$A_3 = \frac{\rho(1-\phi)E + \alpha\phi C_o}{\phi(\alpha + \lambda(K_p + 1))} \tag{A13}$$

$$B_1 = \frac{r}{s}\left(A_2 e^{-rH} - A_1 e^{rH}\right) \tag{A14}$$

$$B_2 = \frac{\rho(1-\phi)E}{\lambda\phi(1 + K_p)} \tag{A15}$$

Model parameters are presented in Table 5.

The benthic flux of each isotope was computed from the modeled pore water profiles. The total seafloor isotope flux ($J_{SF}$) is the sum of two components, a diffusive flux ($J_d$) and an irrigation flux ($J_i$):

$$J_{SF} = L(J_d + J_i) = L\left[-\phi D_s\left(\frac{\partial C}{\partial z}\right)_{z=0} - \alpha\phi\int_o^H (C - C_o)dz\right] \tag{A16}$$

where $L$ is the distance between the shoreline and where the mixed layer base intersects the seafloor, and the other terms are as defined above. The negative sign represents a flux out of the sediments.

The flux ratios for the diffusive and irrigation components of the total flux are different and are sensitive to the irrigation rate. To show this, a simplified estimate of the Ra distribution in the upper zone (Eq. (A7)) can be made. First, since $\lambda C_{eq}$ is orders of magnitude larger than the Ra concentration in overlying water, $C_o = 0$. Second, assuming irrigation is deep relative to the diffusive scale length, Eq. (A11) reduces to $A_1 = 0$. Then, for $z < H$:

$$C(z) = C_{irr}(1 - e^{-rz}) \tag{A17}$$

where $r$ is as defined above and

$$C_{irr} = \rho(1-\phi)E/\left[\phi(\alpha + \lambda(K_p + 1))\right] \tag{A18}$$

Physically, $C_{irr}$ is the average concentration in the irrigated zone. The total flux and its components can then be computed:

$$J_{tot} = J_{diff} + J_{irr} = -\left(\frac{\rho(1-\phi)E}{\phi}\right)\sqrt{\frac{D_s}{\alpha + \lambda(K_p + 1)}} - \alpha\phi\frac{\rho(1-\phi)Ez_{irr}}{\phi\left[\alpha + \lambda(K_p + 1)\right]} \tag{A19}$$

From this equation, it is clear that both the diffusive flux and the irrigation flux depend on $\alpha$. In addition, the relative importance of each component will depend on $\alpha$. In a diffusive system, $\alpha = 0$ and $J_{irr} = 0$. As $\alpha >> \lambda$, $J_{dif} \approx 0$ and $J_{irr} = \rho(1-\phi)Ez_{irr}$. Similarly, the contribution of $J_{diff}$ and $J_{irr}$ to the $^{224}Ra/^{223}Ra$ flux ratio will depend on $\alpha$. For $\alpha << \lambda$, the flux ratios are:

$$R_{J\text{irr}} = \left(\frac{J_{224}}{J_{223}}\right)_d = \frac{E_{224}}{E_{223}}\sqrt{\frac{\lambda_{223}}{\lambda_{224}}} \tag{A20}$$

$$R_{J\text{irr}} = \left(\frac{J_{224}}{J_{223}}\right)_i = \frac{E_{224}}{E_{223}}\frac{\lambda_{223}}{\lambda_{224}} \tag{A21}$$

However, at low irrigation rates, $J_{tot} \approx J_{dif}$, so $R_{Jtot} \approx R_{Jdif}$, but as $\alpha \approx \lambda$, this difference in the flux ratios becomes increasingly important, and $R_{Jtot}$ is bounded by $R_{Jdiff}$ and $R_{Jirr}$. Finally, as $\alpha >> \lambda$, $R_{Jtot} = E_{224}/E_{223}$.

## References


Aller, R.C., 2001. Transport and reactions in the bioirrigated zone. In: Boudreau, B.P., Jørgensen, B.B. (Eds.), The Benthic Boundary Layer: Transport processes and biogeochemistry. Oxford University Press, New York, pp. 269–295.

Bascom, W.N., 1951. The relationship between sand size and beach-face slope. Trans. Amer. Geophys. Union 32, 866–874.

Boehm, A., Paytan, A., Shellenbarger, G.G., Davis, K.A., 2006. Composition and flux of groundwater from a California beach aquifer: implications for nutrient supply to the surf zone. Cont. Shelf Res. 26 (2), 269–282.

Boudreau, B.P., 1984. On the equivalence of nonlocal and radial-diffusion models for pore water irrigation. J. Mar. Res. 42, 731–735.

Brennan, P., 2003. Sea intruding on O.C. groundwater supply. Orange County Register, Santa Ana, CA.

Broecker, W.S., 1965. The application of natural radon to problems in ocean circulation. In: Ichiye, T. (Ed.), Symposium on Diffusion in Oceans and Fresh Waters. Lamont-Doherty Geological Observatory, Palisades, NY, pp. 116–145.

Colbert, S.L., 2004. Radium isotopes in San Pedro Bay, CA: Constraint on inputs and use of nearshore distribution to compute nearshore dispersion rates. Ph.D. Thesis, U. Southern California, Los Angeles, CA, 280 pp.

Colbert, S.L., Hammond, D.E., 2007. Temporal and spatial variability of Ra in the coastal ocean and its impact on computation of nearshore cross-shelf mixing rates. Cont. Shelf Res. doi:10.1016/j.csr.2007.01.003.

Denny, M.W., 1988. Biology and the Mechanics of the Wave-Swept Environment. Princeton University Press, Princeton, NJ. 344 pp.

Drake, D.E., Cacchione, D.A., Karl, H.A., 1985. Bottom currents and sediment transport on San Pedro Shelf, California. J. Sediment. Petrol. 55 (1), 15–28.

Emerson, S., Jahnke, R., Heggie, D., 1984. Sediment-water exchange in shallow-water estuarine sediments. J. Mar. Res. 42, 709–730.

Emery, K.O., 1960. The sea off Southern California. John Wiley and Sons, New York. 366 pp.

Emery, K.O., Foster, J.F., 1948. Water tables in marine beaches. J. Mar. Res. 7, 644–654.

Felix, D.W., Gorsline, D.S., 1971. Newport Canyon, California: an example of the effects of shifting loci of sand supply on canyon position. Mar. Geol. 10, 177–198.

Gorsline, D.S., Grant, D.J., 1972. Sediment textural patterns on the San Pedro shelf, California (1951-1971): Reworking and transport by waves and currents. In: Swift, D.J.P., Duane, D.B., Pilkey, O.H. (Eds.), Shelf Sediment Transport: Process and Pattern. Dowden, Hutchinson & Ross, Stroudsburg, PA.

Grant, D.J., 1973. Sediments of the San Pedro Shelf. Masters Thesis, U. Southern California, Los Angeles, CA, 93 pp.

Hammond, D.E., Fuller, C., 1979. The use of radon-222 to estimate benthic exchange and atmospheric exchange rates in San Francisco Bay. In: Conomos, T.J. (Ed.), San Francisco Bay: The Urbanized Estuary. Pacific Div. Amer. Assoc. Adv. Sci. , pp. 213–230.

Hancock, G.J., Webster, I.T., Ford, P.W., Moore, W.S., 2000. Using Ra isotopes to examine transport processes controlling benthic fluxes into a shallow estuarine lagoon. Geochim. Cosmochim. Acta. 64 (21), 3685–3699.

Herndon, R.L., 1992. Hydrogeology of the Orange County groundwater basin — an overview. In: Heath, E.G., Lewis, W.L. (Eds.), The Regressive Pleistocene Shoreline: Coastal Southern California. Field Trip Guide Book. South Coast Geological Society, Los Angeles, pp. 237–259.

Horrer, P.L., 1950. Southern hemisphere swell and waves from a tropical storm at Long Beach, California. U.S. Army Corps of Engineers, Beach Erosion Board 4 (3), 1–18.

Huettel, M., Rusch, A., 2000. Transport and degradation of phytoplankton in permeable sediment. Limnol. Oceanogr. 45 (3), 534–549.

Huettel, M., Webster, I.T., 2001. Porewater flow in permeable sediments. In: Boudreau, B.P., Jørgensen, B.B. (Eds.), The Benthic Boundary Layer: Transport processes and biogeochemistry. Oxford University Press, New York, pp. 144–179.

Huettel, M., Ziebis, W., Forster, S., 1996. Flow-induced uptake of particulate matter in permeable sediments. Limnol. Oceanogr. 41, 309–322.

Imboden, D.M., 1981. Tracers and mixing in the aquatic environment: A critical discussion of diffusion models and an introduction into concepts of non-Fickian transport. Ph.D. Thesis, Swiss Federal Institute of Technology, 137 pp.

Jähne, B., Heinz, G., Dietrich, W., 1987. Measurement of the diffusion coefficients of sparingly soluble gases in water. J. Geophys. Res. 92 (C10), 10767–10776.

Jahnke, R.A., Nelson, J.R., Marinelli, R.L., Eckman, J.E., 2000. Benthic flux of biogenic elements on the Southeastern U.S. continental shelf: Influence of pore water advective transport and benthic microalgae. Cont. Shelf Res. 20, 109–127.

Karl, H.A., Cacchione, D.A., Drake, D.E., 1980. Erosion and transport of sediments and pollutants in the benthic boundary layer on the San Pedro Shelf, Southern California. U.S. Geological Survey Open File Report, pp. 80–386. 54 pp.

Krishnaswami, S., Graustein, W.C., Turekian, K.K., Dowd, J.F., 1982. Radium, thorium and radioactive lead isotopes in groundwaters: application to the in situ determination of adsorption-desorption rate constants and retardation factors. Water Res. Res. 18 (6), 1633–1675.

Krishnaswami, S., Seidemann, D.E., 1988. Comparative study of 222Rn, 40Ar, 39Ar, and 37Ar leakage from rocks and minerals: implications for the role of nanopores in gas transport through natural silicates. Geochim. Cosmochim. Acta 52 (3), 655–658.

Li, Y.-H., Gregory, S., 1974. Diffusion of ions in seawater and in deep-sea sediments. Geochim. Cosmochim. Acta 38, 703–714.

Magnusen, C.E., 1995. The characterization of Huntington Beach and Newport Beach through fourier grain-shape, grain-size, and longshore current analyses. Masters Thesis, U. Southern California, Los Angeles, CA, 178 pp.

Mathieu, G.G., Biscaye, P.E., Lupton, R.A., Hammond, D.E., 1988. System for measurement of 222Rn at low levels in natural waters. Health Physics 55 (6), 989–992.

McLachlan, A., 1979. Volumes of sea water filtered by East Cape sandy beaches. S. Afr. J. Sci. 75, 75–79.

McLachlan, A., 1982. A model for the estimation of water filtration and nutrient regeneration by exposed sandy beaches. Mar. Envir. Res. 6, 37–47.

Moore, D.G., 1951. The marine geology of San Pedro Shelf. Masters Thesis, U. Southern California, Los Angeles, CA, 87 pp.

Moore, W.S., 1976. Sampling radium-228 in the deep ocean. Deep-Sea Res. 23, 647–651.

Moore, W.S., 2000a. Ages of continental shelf waters determined from 223Ra and 224Ra. J. Geophys. Res. 105C (9), 22117–22122.

Moore, W.S., 2000b. Determining coastal mixing rates using radium isotopes. Cont. Shelf Res. 20, 1993–2007.

Moore, W.S., Arnold, R., 1996. Measurement of 223Ra and 224Ra in coastal waters using a delayed coincidence counter. J. Geophys. Res. 101, 1321–1329.

Mu, Y.K., Cheng, A.H.D., Badiey, M., Bennett, R., 1999. Water wave driven seepage in sediment and parameter inversion based on pore pressure data. Int. J. Num. Anal. Methods Geomech. 23, 1655–1674.

Noble, M., 2003. Huntington Beach shoreline contamination investigation, phase III. U.S. Geological Survey Open File Report 03-62.

Precht, E., Huettel, M., 2003. Advective pore-water exchange driven by surface gravity waves and its ecological implications. Limnol. Oceanogr. 48, 1674–1684.

Rama, Moore, W.S., 1984. Mechanism of transport of U–Th series radioisotopes from solids into ground water. Geochim. Cosmochim. Acta 48 (2), 395–400.

Rama, Moore, W.S., 1996. Using the radium quartet for evaluating groundwater input and water exchange in salt marshes. Geochim. Cosmochim. Acta. 60 (23), 4645–4652.

Riedl, R.J., 1971. How much seawater passes through sandy beaches? Revue fes. Hydrobiol. 56, 923–946.

Riedl, R.J., Huang, N., Machan, R., 1972. The subtidal pump: a mechanism of interstitial water exchange by wave action. Mar. Biol. 13, 210–221.

Sun, Y.I., Torgersen, T., 2001. Adsorption–desorption reactions and bioturbation transport of 224Ra in marine sediments: a one-dimensional model with applications. Mar. Chem. 74, 227–243.

Torgersen, T., et al., 1996. $^{224}$Ra distribution in surface and deep water of Long Island Sound: sources and horizontal transport rates. Cont. Shelf Res. 16 (12), 1545–1559.

Townsend, T.H., 1997. Numerical simulations of tracer loss from benthic chambers: An investigation of bio-irrigation rates and patterns in marine sediments. Masters Thesis, University of Southern California, Los Angeles, CA, 173 pp.

Ullman, W.J., Aller, R.C., 1982. Diffusion coefficients in nearshore marine sediments. Limnol. Oceanogr. 27 (3), 552–556.

Wong, C.S., Chin, Y.-P., Gschwend, P.M., 1992. Sorption of radon-222 to natural sediments. Geochim. Cosmochim. Acta 56 (11), 3923–3932.

Xu, J.P., 2005. Observations of plan-view sand ripple behavior and spectral wave climate on the inner shelf of San Pedro Bay, CA. Cont. Shelf Res. 25, 373–396.

Ziebis, W., Huettel, M., Forster, S., 1996. Impact of biogenic sediment topography on oxygen fluxes in permeable seabeds. Mar. Ecol. Prog. Ser. 140, 227–237.